Multi-Radar Self-Calibration Method using High-Definition Digital Maps for Autonomous Driving

R. Izquierdo, I. Parra, D. Fernández-Llorca and M. A. Sotelo

***Abstract*— Advanced Driving Assistance Systems rely on a very precise sensor-based environmental perception. The quality of the perception depends on the quality of the calibration when multiple and/or redundant sensors are used. This work presents a novel self-calibration method for radars based on high-definition digital maps and high radar-sensitive structural elements. The calibration targets are transformed from the world into the vehicle reference system according to the estimated vehicle state. Then, the calibration between the radar and the vehicle frame is split into two phases, alignment and translation estimation. The alignment is based on the trajectory described by the calibration targets when the vehicle is moving, and the translation is based on position differences when is standing. The uncertainties of the detections are treated in a scoring fashion. Three radars of two different models have been calibrated with this method achieving radar alignments below the angular accuracy and mean range errors below the radar range accuracy.**

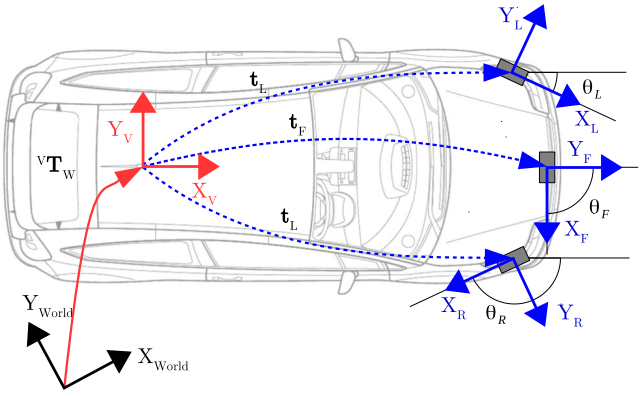

Fig. 1. Radars configuration and systems of reference framework.

I. Introduction and Related Works

Advanced Driving Assistance Systems (ADAS) and autonomous vehicles rely on a very precise sensor-based environmental perception and ego vehicle state estimation. To increase the accuracy and robustness of these systems, multi-modal complementary sensors are used (vision, Lidar, RADAR, IMUs, GPS, etc.). Usually, the accuracy of these sensors depends on extrinsic (position and alignment) and intrinsic parameters that are obtained through, ideally, unsupervised calibration procedures. The quality and long-time stability of these calibrations will establish the quality of the environmental representation and therefore of the autonomous driving decisions.

Consequently, there are numerous publications that address the problem of semi-supervised calibration of one or several sensors onboard autonomous vehicles. Vision systems are probably the most common given the amount of information they provide and their low-cost [1]. In the recent years, also laser scanners have become very popular, due to the rapid development of their technology and the release of new 360° field of view scanners. This has led to the development of vision-laser extrinsic semi-supervised calibration methods [2] [3]. However, there are not that many works devoted to the extrinsic calibration of RADAR sensors. RADAR sensors are commonly used in the automotive industry for Collision Warning/Avoidance (CW/A), Adaptive Cruise Control (ACC) or Parking Assistance systems. Most of these applications are used to monitor traffic surrounding the vehicle, only needing a conservative estimation of other road participants position and speed. Automotive RADARs usually can adjust the elevation plane through semi-supervised calibration procedures that involve the use of a known reflective target at a predefined position. More advanced systems allow for a self-calibration of the azimuth angle or alignment using static targets tracked during a *calibration sequence*. These self-calibration procedures are intended for maintenance/repair of ADAS such as Adaptive Cruise Control (ACC).

However, for autonomous driving applications which require integrating perception information with a digital map to create a representation of the environment [4] [5], the extrinsic calibration of the sensors to the vehicle frame is a significant problem. An alignment error of just 1° can introduce a lateral offset of ∼2 m at 100 m for a RADAR system. This error will make difficult to associate targets to its correct lane. In [6] a millimeter-wave RADAR is mounted on top of a vehicle to scan the surroundings of the vehicle. The RADAR is calibrated using a Radar-Centric Ground Detection (RCGD) that allows the system to estimate the ground elevation and thus reject false detections due to ground detections. In [7] a RADAR mounted in the front of a vehicle is calibrated using a sequence of stationary objects while driving on an approximately straight line. The alignment is estimated using the average velocity profile of the targets, compensating the angular movement with an IMU.

In this paper, we propose an alignment algorithm for multiple RADARs onboard a vehicle (see fig. 1). The procedure takes advantage of a high definition digital map used

R. Izquierdo, I. Parra, D. Fernández-Llorca and M. A. Sotelo are with the Computer Engineering Department, University of Alcalá, Alcalá de Henares, Spain ruben.izquierdo@uah.es

for autonomous navigation to provide the precise location of stationary objects (street lamps and traffic signs). Using the positions of the calibration targets while the vehicle is moving and standing the calibration procedure computes the azimuth angle and translation with respect to the vehicle frame. This method allows online self-calibration of the RADARs without special tools or needing to take the vehicle to the Original Equipment Manufacturer (OEM). Our method would allow the autonomous vehicle to be programmed to regularly perform auto-calibrations of the RADARs based on the information of a high definition digital map and the RADARs acquired targets.

The remainder of the paper is organized as follows: Section II describes the propagation of the radar error detections. The radars calibration procedure is exposed in Section III. Experimental results are presented and discussed in Section IV, and finally, conclusions and future works are addressed in Section V.

II. Radar Error Propagation

The radar detection accuracy is in general provided in a polar reference system just like the measures are. On many occasions the positions are transformed to an orthonormal reference system according to eq. 1, where ρ is the detection range, α is the direction of the detection and x and y are the orthonormal coordinates. The error of the orthonormal coordinates is propagated as follows:

$$x = \rho\cos(\alpha), \quad y = \rho\sin(\alpha) \tag{1}$$

$$\frac{\partial x}{\partial \rho} = \cos(\alpha), \quad \frac{\partial y}{\partial \rho} = \sin(\alpha) \tag{2}$$

$$\frac{\partial x}{\partial \alpha} = -\rho\sin(\alpha), \quad \frac{\partial y}{\partial \alpha} = \rho\cos(\alpha) \tag{3}$$

Assuming the range error ε_ρ and the direction error ε_α are independent variables the errors ε_x and ε_y can be computed as it is shown in eqs. 4 and 5.

$$\varepsilon_x = \sqrt{\left(\frac{\partial x}{\partial \rho}\varepsilon_\rho\right)^2 + \left(\frac{\partial x}{\partial \alpha}\varepsilon_\alpha\right)^2} \tag{4}$$

$$\varepsilon_y = \sqrt{\left(\frac{\partial y}{\partial \rho}\varepsilon_\rho\right)^2 + \left(\frac{\partial y}{\partial \alpha}\varepsilon_\alpha\right)^2} \tag{5}$$

In our case, the position accuracy is limited due to the CAN bus communication protocol. The position of the objects has a resolution of 0.1 m, which limits the position error to a minimum value as it is expressed in eq. 6.

$$\varepsilon_x = \max\{0.1, \varepsilon_x\}, \quad \varepsilon_y = \max\{0.1, \varepsilon_y\} \tag{6}$$

When two detections i, j are used to compute the direction of the vector formed by them by using the arctan function, the errors of both detections are involved in the error of the resulted direction. Eqs. from 7 to 11 describe the computation of the direction error based on the points errors.

$$\theta = \arctan(\Delta y/\Delta x) \tag{7}$$

$$\frac{\partial \theta}{\partial \Delta x} = \frac{-1}{\Delta y + \Delta x^2/\Delta y} \tag{8}$$

$$\frac{\partial \theta}{\partial \Delta y} = \frac{1}{\Delta x + \Delta y^2/\Delta x} \tag{9}$$

Assuming $\varepsilon_{\Delta x}$ and $\varepsilon_{\Delta y}$ are independent variables the direction error ε_θ can be computed as follows:

$$\varepsilon_\theta = \sqrt{\left(\frac{\partial \theta}{\partial \Delta x}\varepsilon_{\Delta x}\right)^2 + \left(\frac{\partial \theta}{\partial \Delta y}\varepsilon_{\Delta y}\right)^2} \tag{10}$$

$$\varepsilon_{\Delta x} = \varepsilon_{x_i} + \varepsilon_{x_j}\ ,\ \varepsilon_{\Delta y} = \varepsilon_{y_i} + \varepsilon_{y_j} \tag{11}$$

III. Calibration Procedure

The calibration procedure tries to estimate the transformation matrix ${}^{\mathrm{V}}\mathbf{T}_{\mathrm{R}}$ that transforms points from the radar reference system $\mathrm{S_R}$ to the vehicle reference system $\mathrm{S_V}$. In the case of more than one radar, the transformation matrix allows to transform points from one radar to each other in a common frame, and thus the generation of continuous trajectories.

$$\mathrm{S_V} = {}^{\mathrm{V}}\,\mathbf{T}_{\mathrm{R}}\mathrm{S_R} \tag{12}$$

Any transformation matrix $\mathbf{T}$ can be splitted in two basic spatial operations, a rotation $\mathbf{R}_{2\times2}$ and a trastlation $\mathbf{t}_{2\times1}$.

$$\mathbf{T} = \begin{bmatrix} \mathbf{R}_{2\mathrm{x}2} & \mathbf{t}_{2\mathrm{x}1} \\ \mathbf{0}_{1\mathrm{x}2} & 1 \end{bmatrix} \tag{13}$$

The calibration procedure splits the estimation of the transformation matrix in two steps, the first one estimates the rotation matrix and the second one the translation vector.

A. Calibration Environment Description

The calibration method exploits the detection of high radar-sensitive structural elements which are static and their location is fixed in a global reference system. The calibration environment consists of two ways road with two lanes per way with a roundabout at each end. There is a sidewalk with street lights and traffic signs on both sides of the road. The street lights and the traffic signs positions have been used as targets in the calibration procedure. Their positions have been measured with a Differential Global Navigation Satellite System (DGNSS) with an error lower than 2 cm. The higher the quality of the elements in the environment the better the calibration is. The recorded positions are surrounding to the vertical pole axis, so the pole axis position is estimated as the centroid of the measures. The latitude-longitude coordinates are transformed into an easting-northing reference system according to the transverse Mercator projection in order to get a flat and orthonormal representation reference system. Fig. 2 shows the position of some of the street lights and the traffic signs in a high definition digital map representation of the environment.

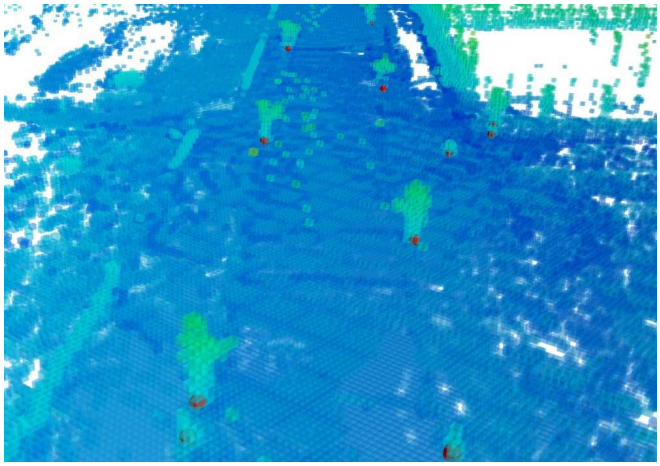

Fig. 2. Calibration targets in a digital map. Red spheres represent the GPS coordinates of the calibration elements.

B. Ego-Position Estimation

An Extended Kalman Filter (EKF) has been used to fuse the information from a DGNSS with Real Time Kinematic (RTK) accuracy, an MPU6050 Inertial Measurement Unit (IMU) and the Controller Area Network (CAN) bus of the vehicle. The state vector $\hat{x}$ is estimated using the measure vector z, the non linear process model f and the observation model h according to the eqs. described in [8], where E and N are the easting and northing (world) coordinates respectively, ϕ is the heading or forward direction, v is the longitudinal speed and $\dot{v}$ is the longitudinal acceleration.

$$x = \begin{bmatrix} E & N & \phi & v & \dot{\phi} & \dot{v} \end{bmatrix}^T \tag{14}$$

$$z = \begin{bmatrix} E & N & v & \dot{\phi} & \dot{v} \end{bmatrix}^T \tag{15}$$

$$\hat{x}_k = f\left(\hat{x}_{k-1}\right) + w_k, \quad \hat{z} = h\left(\hat{x}_k\right) + v_k \tag{16}$$

In order to transform the position of the calibration elements from the world reference system $\mathrm{S_W}$ to the vehicle (local) reference system $\mathrm{S_V}$ a transformation $\mathbf{T}$ is performed according to the vehicle state vector.

$$\mathrm{S_V} = \mathbf{T}^{-1} \cdot \mathrm{S_W} \tag{17}$$

$$\mathbf{T} = \begin{bmatrix} \cos(\phi) & -\sin(\phi) & E \\ \sin(\phi) & \cos(\phi) & N \\ 0 & 0 & 1 \end{bmatrix} \tag{18}$$

C. Rotation Estimation

The rotation calibration process estimates the radar rotation angle θ_R that aligns the vehicle reference system $\mathrm{S_V}$ and the radar reference system $\mathrm{S_R}$. Matrix $\mathbf{R}$ is a two-dimensional rotation transformation according to eq. 20.

$$\mathrm{S_V} = \mathbf{R}\mathrm{S_R} \tag{19}$$

$$\mathbf{R} = \begin{bmatrix} \cos(\theta_\mathrm{R}) & -\sin(\theta_\mathrm{R}) \\ \sin(\theta_\mathrm{R}) & \cos(\theta_\mathrm{R}) \end{bmatrix} \tag{20}$$

As far as the relation between the radar detections and the targets is not known the traditional calibration approaches based on pairs of points cannot be conducted. An alternative methodology based on the relative movement properties of static objects has been developed. The trajectory described by a static object is seen from the sensor reference system as the opposite of its own trajectory. If the mobile reference system (vehicle) performs a trajectory in a straight line, the trajectory of the static object is seen as a straight line in the opposite direction in the sensor reference system. The orientation of the trajectory in the sensor reference system reveals the rotation needed to virtually align both reference systems.

The trajectories generated by the objects are a sequence of points in the radar reference system $\mathrm{S_R}$. A single trajectory P is formed by a set of n points p as it is defined in eq. 21, where the subindex represents the time-order of the points.

$$\mathrm{P} = \{p_1, p_2, \ldots, p_n\} \tag{21}$$

Assuming that the trajectory represents a straight line the orientation can be easily computed as the arctan function of the extreme points. However, due to the radar detection accuracy, this way is not the best. The endpoints of the trajectory are commonly in the border of the detection area, which is where the detection error is higher. A set of tuples of points TP associated to the trajectory P is defined in eq. 21, which generates all the possible combinations of points in the trajectory P in a forward time sense.

$$\mathrm{TP} = \{(p_i, p_j) \mid p_i, p_j \in \mathrm{P},\ p_i \neq p_j,\ i < j\} \tag{22}$$

The trajectory direction θ is computed for each tuple of points in TP according to eq. 7. The error asociated to each computed direction ε_θ depens on the individual point errors. The orientation error formula is described in section II, eqs. from 7 to 11.

At this point, many rotations and their associated errors have been computed for each trajectory P. Now, the trajectories described by many detections must be commonly evaluated in order to achieve the most reliable value of $\hat{\theta}$. Four different functions are proposed to evaluate the set of rotations and errors in a scoring fashion as they are described below. The shape of the scoring functions is shown in fig. 3.

- The first score function s_1 is a normal distribution $\mathcal{N}(\mu, \sigma^2)$ with mean value $\mu = \theta$ and standard deviation $\sigma = \varepsilon_\theta$. The 68.27% of the score is concentrated in a band of $2\varepsilon_\theta$ centered in θ.

$$s_1(\hat{\theta}, \theta, \varepsilon_\theta) = \mathcal{N}\left(\theta, {\varepsilon_\theta}^2\right) \tag{23}$$

- The second score function s_2 is a truncated version of s_1. This function assigns the same score $\overline{s}_2$ to the estimated orientation range in the uncertainty band.

$$s_2(\hat{\theta}, \theta, \varepsilon_\theta) = \begin{cases} \overline{s}_2 & |\theta - \hat{\theta}| \leq \varepsilon_\theta \\ s_1(\hat{\theta}, \theta, \varepsilon_\theta) & \text{otherwise.} \end{cases} \tag{24}$$

$$\overline{s}_2 = s_1(\varepsilon_\theta, \theta, \varepsilon_\theta) \tag{25}$$

- The third score function s_3 implements a linear version of the normal distribution function. The function is centered in θ and the score decreases with a constant

value K. In order to generate a cumulative score of 1, the maximum score A and the slope K are computed according to eqs. 27 and 28.

$$s_3(\hat{\theta},\theta,\varepsilon_\theta) = \begin{cases} A - K|\theta - \hat{\theta}| & |\theta - \hat{\theta}| \leq 2\varepsilon_\theta \\ 0 & \text{otherwise.} \end{cases} \quad (26)$$

$$A = 1/4{\varepsilon_\theta}^2 \quad (27)$$

$$K = 1/4{\varepsilon_\theta}^2 \quad (28)$$

- The fourth score function s_4 implements a truncated version of s_3. This function assigns the same score $\overline{s}_4$ to the estimated orientation in the uncertainty band.

$$s_4(\hat{\theta},\theta,\varepsilon_\theta) = \begin{cases} \overline{s}_4 & |\theta - \hat{\theta}| \leq \varepsilon_\theta \\ s_3(\hat{\theta},\theta,\varepsilon_\theta) & \text{otherwise.} \end{cases} \quad (29)$$

$$\overline{s}_4 = s_3(\varepsilon_\theta,\theta,\varepsilon_\theta) \quad (30)$$

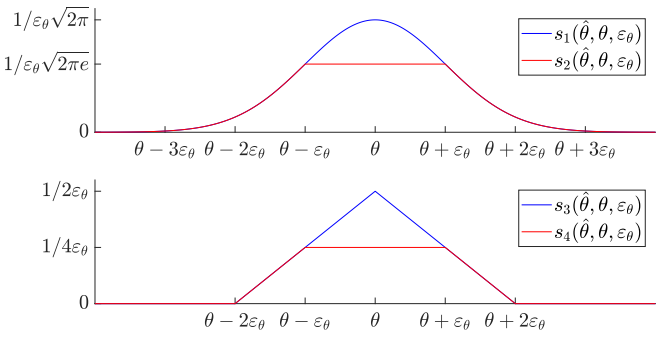

Fig. 3. Rotation scoring functions. s_1 and s_2 on top and s_3 and s_4 on bottom.

The global score is computed as the sum of each individual score distribution according to eq. 31, where s is one of the four scoring functions and n is the total number of scored angles. The total score distribution is normalized in order to be treated as a probability density function and to provide a confidence interval of the estimations.

$$S(\hat{\theta}) = \sum_{i=1}^{n} s(\hat{\theta},\theta_i,\varepsilon_{\theta_i}) \quad (31)$$

Finally, the radar rotation angle θ_R is minus the $\hat{\theta}$ value with the highest cumulative score according to eq. 32 due to the opposite direction of the relative object's movement.

$$-\theta_\mathrm{R} = \underset{\hat{\theta}\,\in\,(-2\pi,2\pi]}{\operatorname{argmax}} \; S(\hat{\theta}) \quad (32)$$

D. Translation Estimation

Once the rotation between the vehicle and the radar reference systems is known and they are virtually aligned, the position difference between targets and detections is the translation which is being looked for. The translation estimation has three stages, firstly the world points are transformed to the vehicle reference system, secondly the radar detections are rotated to be aligned with the vehicles reference system, and finally, the vehicle-radar translation is achieved by scoring the individual detection-target translations.

In a first step, the position of the calibration targets is transformed from the world reference system to the vehicle reference system according to eq. 17. In order to avoid time delays between the radar detection and the ego-estimation systems, static sequences are used to calibrate the translation.

In the second step, the radar detections and their errors are rotated to be aligned with the vehicle reference system according to eq. 19.

A two-dimensional translation vector $\mathbf{t}$ defined in eq. 33 is needed to transform calibration targets to detections in the common vehicle reference system and vice-versa. The parameters that need to be found are t_x and t_y which are the translation along the x and the y axis of the vehicle respectively.

$$\mathbf{t} = \begin{bmatrix} t_x \\ t_y \end{bmatrix} \quad (33)$$

The translation vector $\mathbf{t}$ has been limited by using basic information of the vehicle dimensions. The translation vector limit $\mathbf{t}_L$ is defined in equation 34 where W and L are the width and length of the vehicle and δ_x and δ_y a safety gap to avoid possible exclusions due to the radar detection errors.

$$\mathbf{t}_\mathrm{L} = \begin{bmatrix} L + \delta_x \\ W + \delta_y \end{bmatrix} \quad (34)$$

The set of translation vectors TV is defined in eq. 36 as all the combination of translation vectors $\mathbf{t}_{i,j}$ for each radar detection d_i to each calibration target ct_j. The translation vector is computed as it is shown in eq. 35. If $\mathbf{t}_{i,j}$ exceeds $\mathbf{t}_\mathrm{L}$ the pair d_i and ct_j is assumed as a wrong matching and consequently is excluded from the translation estimation process.

$$\mathbf{t}_{i,j} = ct_j - d_i \quad (35)$$

$$\mathrm{TV} = \{\mathbf{t}_{i,j} \mid -\mathbf{t}_\mathrm{L} \leq \mathbf{t}_{i,j} \leq \mathbf{t}_\mathrm{L},\ \forall i,j\} \quad (36)$$

The error asociated to each translation $\boldsymbol{t}_{i,j}$ is defined as the error vector $\boldsymbol{\varepsilon}_{t_i} = (\varepsilon_{x_i}, \varepsilon_{y_i})$ which is the result of the detection error rotation.

Equivalently for the radar rotation, four bi-dimensional scoring functions have been designed to find out the radar translation. The shape of the scoring functions is shown in fig. 4.

- The first score function s_5 is a normal distribution $\mathcal{N}(\mu,\sigma^2)$ with mean value $\mu = \mathbf{t}$ and standard deviation $\sigma = \boldsymbol{\varepsilon}_t$.

$$s_5(\hat{\mathbf{t}},\mathbf{t},\boldsymbol{\varepsilon}_t) = \mathcal{N}\left(\mathbf{t},{\boldsymbol{\varepsilon}_t}^2\right) \quad (37)$$

- The second score function s_6 is a truncated version of s_5. The same score $\overline{s}_6$ is assigned to the translations inside the uncertainty band. In equation 38 operation $./$ represents the element-wise division.

$$s_6(\hat{\mathbf{t}},\mathbf{t},\boldsymbol{\varepsilon}_t) = \begin{cases} \overline{s}_6 & \|(\mathbf{t} - \hat{\mathbf{t}})./\boldsymbol{\varepsilon}_t\| \leq 1 \\ s_5(\hat{\mathbf{t}},\mathbf{t},\boldsymbol{\varepsilon}_t) & \text{otherwise.} \end{cases} \quad (38)$$

$$\overline{s}_6 = s_5((\varepsilon_{t_x},0) + \mathbf{t},\mathbf{t},\boldsymbol{\varepsilon}_t) \quad (39)$$

- The third score function s_7 implements a linear version of s_5. The score decreases according to $\mathbf{K}$ around $\mathbf{t}$. The matrix $\mathbf{K}$ and the maximum value A are computed acording to eqs. 41 and 42 in order to achieve a cumulative score of 1. The function max is the vectorial maximum.

$$s_7(\hat{\mathbf{t}}, \mathbf{t}, \boldsymbol{\varepsilon}_t) = \begin{cases} A - \max\left(\mathbf{K}|\mathbf{t} - \hat{\mathbf{t}}|\right) & |\mathbf{t} - \hat{\mathbf{t}}| \leq 2\boldsymbol{\varepsilon}_t \\ 0 & \text{otherwise.} \end{cases} \tag{40}$$

$$A = 3/16\varepsilon_{t_x}\varepsilon_{t_y} \tag{41}$$

$$\mathbf{K} = \frac{3}{32}\begin{bmatrix} 1/\varepsilon_{t_x}^2\varepsilon_{t_y} & 0 \\ 0 & 1/\varepsilon_{t_x}\varepsilon_{t_y}^2 \end{bmatrix} \tag{42}$$

- The fourth score function s_8 implements a truncated version of s_7. This function assigns the same score $\overline{s}_8$ to the estimated translation in the uncertainty band like the score function s_6.

$$s_8(\hat{\mathbf{t}}, \mathbf{t}, \boldsymbol{\varepsilon}_t) = \begin{cases} \overline{s}_8 & |\mathbf{t} - \hat{\mathbf{t}}| < \boldsymbol{\varepsilon}_t \\ s_7(\hat{\mathbf{t}}, \mathbf{t}, \boldsymbol{\varepsilon}_t) & \text{otherwise.} \end{cases} \tag{43}$$

$$\overline{s}_8 = s_7(\boldsymbol{\varepsilon}_t + \mathbf{t}, \mathbf{t}, \boldsymbol{\varepsilon}_t) \tag{44}$$

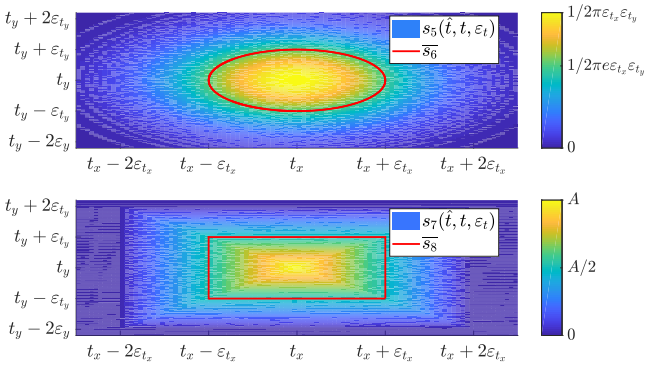

Fig. 4. Translation scoring functions. On top s_5 and s_6, on bottom s_7 and s_8. Inner area of red ellipse has a constant score of $\overline{s}_6$ in s_6, inner area of the red rectangle has a constant score of $\overline{s}_8$ in s_8.

Finally, the global translation score is computed as the sum of each single translation score function as it is shown in eq. 45 where s is one of the four scoring functions and n is the total number of valid detection-target translations.

$$S\left(\hat{\mathbf{t}}\right) = \sum_{i=1}^{n} s\left(\hat{\mathbf{t}}, \mathbf{t}_i, \boldsymbol{\varepsilon}_{t_i}\right) \tag{45}$$

The estimated radar translation vector $\mathbf{t}$ is achieved finding the translation vector $\hat{\mathbf{t}}$ with the highest S score inside the translation limits $\mathbf{t}_\mathrm{L}$ according to eq. 46.

$$\mathbf{t} = \underset{-\mathbf{t}_\mathrm{L} \leq \hat{\mathbf{t}} \leq \mathbf{t}_\mathrm{L}}{\operatorname{argmax}} \; S\left(\hat{\mathbf{t}}\right) \tag{46}$$

IV. Results

In this section, the final results are shown and commented. The radars which have been calibrated with the proposed method are a long-range radar ARS-308 and two short-range radar SRR-208 located according to the distribution showed in fig. 1. Each radar model has a different error configuration (see table I). The ARS has a range up to 200 m, this fact makes this radar highly sensitive to alignment errors, on the top, the angular accuracy is really high in the narrow beam. In the opposite the SRR has a range up to 50 m, it makes the radar less sensitive to the alignment errors, however, the angular accuracy is lower.

TABLE I
Radar Measuring Performance

	Measuring		min e	e_r	
ARS-308	Distance Accuracy		0.25	1.5%	[m]
	Angle Accuracy	@FoV ±8.5°	0.1		[deg]
		@FoV ±28°	1.0		[deg]
SRR-208	Distance Accuracy		0.2		[m]
	Angle Accuracy	@FoV ±20°	2.0		[deg]
		@FoV ±60°	4.0		[deg]
		@FoV ±75°	5.0		[deg]

For the rotation estimation two different sequences have been recorded, one traveling at 20 km/h and other at 50 km/h. Table II shows the angle estimation and the value that covers the 68.27% of the score for the three radars (units expressed in radians). The recorded sequences have 447 and 301 objects trajectories for ASR-308, 47 and 53 for the SRR208-L and 56 and 65 for the SRR208-R at 20 and 50 km/h respectively.

TABLE II
Radar Rotation Results at 20 and 50 km/h

Scoring fcn.	s_1	s_2	s_3	s_4
20 km/h				
ASR308	1.570±0.036	1.570±0.038	1.569±0.034	1.570±0.036
SRR208-L	0.190±0.057	0.175±0.064	0.194±0.051	0.175±0.058
SRR208-R	2.776±0.054	2.757±0.063	2.777±0.048	2.757±0.056
50 km/h				
ASR308	1.572±0.033	1.571±0.034	1.571±0.030	1.571±0.032
SRR208-L	0.198±0.083	0.184±0.087	0.201±0.078	0.181±0.083
SRR208-R	3.005±0.074	3.013±0.079	3.004±0.070	3.014±0.074

Analyzing the rotation estimations, in general, the non-truncated scoring functions (s_1 and s_3) generate a narrower confidence band, being the narrowest one achieved with the scoring function s_3. Analyzing the effect of the speed, higher speeds produce trajectories with fewer points, this produces different effects depending on the radar. The effects to the ASR are beneficial because the points are more apart but inside the high accuracy detection area, the angle accuracy rises and produces a narrower confident band. The effects to the SRR are not beneficial, the points are more apart but in low accuracy detection areas, generating wider bands.

For the estimation of the translation, 22 static poses have been recorded. There are a total of 74 valid calibration targets for the ARS, 35 for the SRR-L and 33 for the SRR-R. For our particular case, the translation matrix limits $\mathbf{t}_{\mathrm{L}}$ have been set according to the vehicle dimensions $W = 1.79$ m, $L = 4.33$ m and $\delta_x = 2\delta_y = 1.0$ m. The Mean Range Error (MRE) and the Mean Angular Error (MAE) are used as metrics to show the performance of the overall calibration. The translation estimations have a strong dependence with the estimated rotation, therefore a combination of rotation and translation scoring functions pairs are evaluated independently and the results are shown in table III, where the MRE is expressed in percentaje or meters and the MAR is in degrees.

TABLE III
MEAN RANGE ERROR & MEAN ANGULAR ERROR

Scoring fcn		s_1	s_2	s_3	s_4
ASR308	s_5	0.20|0.50	0.20|0.51	0.20|0.52	0.20|0.51
[%]|[deg]	s_6	0.20|0.48	0.19|0.49	0.19|0.50	0.19|0.49
	s_7	0.25|0.52	0.24|0.52	0.23|0.53	0.24|0.52
	s_8	0.60|0.46	0.62|0.46	0.64|0.47	0.62|0.46
SSR208-L	s_5	0.10|1.17	0.12|1.26	0.10|1.14	0.12|1.26
[m]|[deg]	s_6	0.11|2.16	0.15|2.34	0.10|2.17	0.15|2.34
	s_7	0.10|1.18	0.12|1.26	0.10|1.15	0.12|1.26
	s_8	0.11|2.37	0.15|2.53	0.10|2.40	0.15|2.53
SSR208-R	s_5	0.13|1.08	0.13|1.05	0.13|1.11	0.13|1.05
[m]|[deg]	s_6	0.11|2.05	0.12|1.91	0.11|2.07	0.12|1.91
	s_7	0.13|1.07	0.13|1.05	0.13|1.09	0.13|1.05
	s_8	0.17|2.32	0.16|2.10	0.17|2.34	0.16|2.10

The ASR achieves an MAE below 0.5° which is greater than the accuracy of the narrow beam but lower than the accuracy of the wide beam. The SRR achieves an MAE close to 1° which is lower than the accuracy of any beam. The truncated functions produce worst results for this kind of radar. It could be caused by the low angular accuracy of the radar. The alignment in conjunction with the translation performs MRE values which are below the range uncertainty for both kinds of radars. Fig. 5 shows an example of the radar detections reconstruction in the vehicle frame.

V. CONCLUSIONS AND FUTURE WORKS

The presented calibration method allows the calibration of multiple radars onboard a vehicle by using high sensitive static structural elements recorded in a high definition digital map. The method calibrates the alignment of the radars and the translation with respect to the vehicle reference system in an automatic and non-supervised way. The sensor alignment achieved is in the order of the angular radar accuracy or below and the reprojection errors after the translation calibration decrease to values lower than the radar detection range accuracy.

As future works, a time-based synchronization between the radar detection system and the vehicle state estimation system would enable the use of moving trajectories as valid calibration trajectories for rotation and translation estimation.

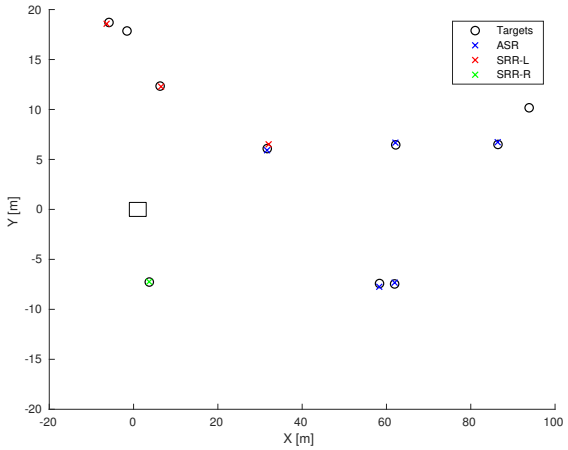

Fig. 5. Radar detections and calibration targets reconstruction in the vehicle reference system. Black square represents the vehicle, black circles are calibration targets, blue x are ASR308 detections, red x are SRR208-L detections and green x are SRR208-R detections.

VI. ACKNOWLEDGEMENTS

This work was funded by Research Grants SEGVAUTO S2013/MIT-2713 (CAM), DPI2017-90035-R (Spanish Min. of Economy), BRAVE Project, H2020, Contract #723021 and FPU14/02694 (Spanish Min. of Education) via a predoctoral grant to the first author. This project has received funding from the Electronic Component Systems for European Leadership Joint Undertaking under grant agreement No 737469 (AutoDrive Project). This Joint Undertaking receives support from the European Unions Horizon 2020 research and innovation programme and Germany, Austria, Spain, Italy, Latvia, Belgium, Netherlands, Sweden, Finland, Lithuania, Czech Republic, Romania, Norway.

REFERENCES

[1] U. Franke, D. Pfeiffer, C. Rabe, C. Knoeppel, M. Enzweiler, F. Stein, and R. G. Herrtwich, "Making bertha see," in *2013 IEEE International Conference on Computer Vision Workshops*, Dec 2013, pp. 214–221.

[2] C. Guindel, J. Beltrán, D. Martín, and F. García, "Automatic extrinsic calibration for lidar-stereo vehicle sensor setups," *CoRR*, vol. abs/1705.04085, 2017. [Online]. Available: http://arxiv.org/abs/1705.04085

[3] D. Gao, J. Duan, X. Yang, and B. Zheng, "A method of spatial calibration for camera and radar," in *2010 8th World Congress on Intelligent Control and Automation*, July 2010, pp. 6211–6215.

[4] R. Izquierdo, I. Parra, J. Munoz-Bulnes, D. Fernández-Llorca, and M. Sotelo, "Vehicle trajectory and lane change prediction using ann and svm classifiers," in *Intelligent Transportation Systems (ITSC), 2017 20th International IEEE Conference on*. IEEE, 2017, pp. 1141–1146.

[5] R. Izquierdo, I. Parra, C. Salinas, D. Fernández-Llorca, and M. Sotelo, "Semi-automatic high-acuracy labelling tool for multi-modal long-range sensor dataset," in *2018 IEEE Intelligent Vehicles Symposium (IV). In press*. IEEE.

[6] G. Reina, D. Johnson, and J. Underwood, "Radar sensing for intelligent vehicles in urban environments," *Sensors*, vol. 15, no. 6, pp. 14 661–14 678, 2015. [Online]. Available: http://www.mdpi.com/1424-8220/15/6/14661

[7] D. Kellner, M. Barjenbruch, K. Dietmayer, J. Klappstein, and J. Dickmann, "Joint radar alignment and odometry calibration," 07 2015.

[8] I. P. Alonso, R. I. Gonzalo, J. Alonso, Á. García-Morcillo, D. Fernández-Llorca, and M. Á. Sotelo, "The experience of drivertive-driverless cooperative vehicle-team in the 2016 gcdc," *IEEE Transactions on Intelligent Transportation Systems*, 2017.